The impact of electron-electron interaction on electron transport in GaAs at high electric fields

1994 J. Phys.: Condens. Matter 6 7027

(http://iopscience.iop.org/0953-8984/6/35/011)

J. Phys.: Condens. Matter 6 (1994) 7027–7044. Printed in the UK

The impact of electron–electron interaction on electron transport in GaAs at high electric fields

Christoph Peschke

Technische Universität Hamburg–Harburg, Arbeitsbereich Hochfrequenztechnik, Wallgraben 55, 21071 Hamburg, Germany

Received 3 March 1994

Abstract. We theoretically investigate the influence of electron–electron interaction and the Pauli exclusion principle on electron transport in highly doped homogeneous n-GaAs. The electron–electron interaction potential is split up into a long- and a short-range part. Electron–electron interaction due to the long-range part is treated as inelastic scattering at coupled plasmon–phonon oscillations; electron scattering processes due to the short-range part are described as elastical collisions of identical particles. The minimal wavelengths of coupled plasmon–phonon oscillations are given by lower limits. Velocity–field characteristics are computed for field strengths of $0 < E \leqslant 30$ kV cm^{-1} and electron concentrations of 10^{16} cm^{-3} and 10^{18} cm^{-3}. A small influence of electron–electron interaction and the Pauli exclusion principle is found at $n = 10^{18}$ cm^{-3}. The large dip in mobility in GaAs at $n = 10^{19}$ cm^{-3} is shown to be caused by the exclusion principle.

1. Introduction

Based on an approach of Bohm and Pines [1], the effect of electron–electron interaction on electron transport in semiconductors can be studied by solving the Boltzmann transport equation using appropriate scattering rates (e.g. [2–4]). These scattering rates account for the energy conserving collision of electrons as well as the interaction of electrons with collective excitations of the electronic electric field. Transition probabilities are computed by time dependent perturbation theory. Scattering rates have also been evaluated using Green functions [5]. Recently, the two approaches have been compared [4], and good agreement has been found. Further work not based on the random phase approximation [1] and the statistical approach to the Pauli principle [3] may keep closer to the Schrödinger equation and adopt ideas covered e.g. in [6] and [7].

The long-range part of the electron–electron interaction has also been treated in a purely classical manner [8]. The electrons are considered to be point charges. The interaction is accounted for by solving the equations for the motion of point charges in the resulting electronic field. In [8] it is shown that the results obtained with this classical molecular dynamics approach differ from the results obtained using the quantum mechanical interaction of electrons with screened potentials and neglecting plasmons. In this paper, we take into account the long-range part of the interaction using the plasmon concept, thus neglecting charge fluctuations. To our knowledge, it is at present hard to say whether a classical description of electron motion using the concept of point charges is closer to reality than a quantum mechanical description accounting for plasmons but neglecting the influence of charge fluctuations on electron motion. We note, however, that it is very difficult to reconcile the plasmon concept with the occurrence of space dependent electron charge distributions,

0953-8984/94/357027+18$19.50

which are also caused by the long-range part of the electron potential. In principle it is possible to construct coherent plasmon states with a non-vanishing expectation value of the resulting electric field [9], thus leading to space dependent charge distributions caused by plasmons.

However, the aim of this paper is not to go beyond the approach based on [1]. Neither do we claim to have solved the problem of simultaneous occurrence of plasmons and charge fluctuations. However, it is not useless to perform an analysis that keeps as close as possible to the basic assumptions of [1]. To our knowledge all investigations of the influence of scattering of electrons at collective electronic excitations introduce additional assumptions to obtain a value for the minimum wavelength of these oscillations. According to [1], the cut-off value can be identified with the minimum wavelength at which a zero of the electronic part of the dielectric function occurs. Hence, the wavelength depends on the electron distribution function. In dynamically determining the minimum value of the wavelength by analysis of the dielectric function, we find that the influence of electron–plasmon scattering on electronic transport is much lower than predicted in [4]. For completeness, we also take into account the coupling of plasmons to polar optical phonons as described in [9]. To sum up, we shall find that plasmons have a very small influence on electron transport, justifying their neglect.

The impact of the exclusion principle on the scattering rates is taken into account by using a rejection technique based on the actual electron distribution [3]. We note that at high electric fields rejection techniques based on Fermi distribution functions clearly overestimate the impact of the Pauli principle.

To separate the influence of each of the effects considered, they are investigated successively. Insofar as our numerical methods deviate from methods applied elsewhere, they are explained in detail. Velocity–field characteristics including all effects are shown. Finally, we investigate the influence of the processes considered on the mobility.

2. The simulation model

The Monte Carlo model used here to simulate electron transport is described in [10]. The detailed formulas for most of the scattering processes can be found in [11]. Any deviations from these expressions are derived in [9] and in the present paper. Our model differs from the previously mentioned ones in the fact that the dependence of several parameters of the scattering rates on the electron distribution function is taken into account.

These parameters are the Thomas–Fermi screening length, the plasma frequency, and the cut-off values of the wave numbers of the plasmon–phonon oscillations. While the latter dependence is discussed in [9] and in subsection 5.1, we now generalize the usual expressions for the screening length and the plasma frequency to the case of a many-valley semiconductor. We derive the screening length following [12] and are led to

$$\beta_{\mathrm{B}}^2 = \frac{e^2}{\varepsilon_{\mathrm{s}} k_{\mathrm{B}}} \sum_{i=1}^{3} \frac{n_i}{T_i} \tag{2.1}$$

if the electrons in all valleys are Boltzmann distributed, and

$$\beta_{\mathrm{F}}^2 = \frac{e^2 m_1^* (3n_1)^{1/3}}{\varepsilon_{\mathrm{s}} \hbar^2 \pi^{4/3}} + \frac{e^2}{\varepsilon_{\mathrm{s}} k_{\mathrm{B}}} \sum_{i=2}^{3} \frac{n_i}{T_i} \tag{2.2}$$

if the electrons in valley 1 (Γ valley) are Fermi distributed. Here β is the inverse of the screening length, e is the elementary charge, ε_{s} is the static permeability, k_{B} is the

Boltzmann constant, n_i is the electron concentration in valley i, m_i^* is the effective mass of an electron in valley i, T_i is the electron temperature in valley i, and $\hbar$ is the Planck constant. The index i denotes the Γ, L, and X valleys, respectively. The electrons in the L and X valleys are always Boltzmann distributed due to the fact that these valleys are only occupied at high electron temperatures. Since at high concentrations $\beta_F < \beta_B$ and at low concentrations $\beta_F > \beta_B$, the screening length is determined from

$$\beta = \min(\beta_B, \beta_F). \tag{2.3}$$

A plot of β versus n (figure 1) for $T = 300$ K, all electrons being in the Γ valley, shows that β_B and β_F intersect at $n \simeq 5 \times 10^{17}$ cm^{-3}, which is near to the electron concentration where the Fermi energy shifts into the conduction band (figure 2).

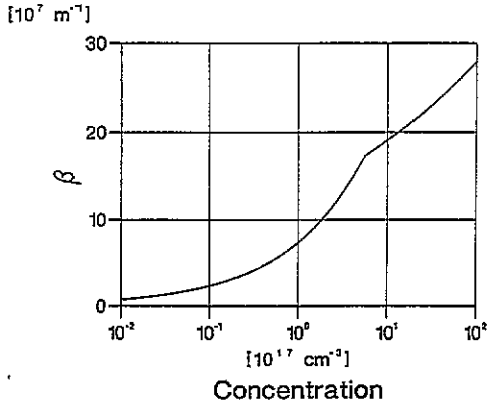

Figure 1. The inverse of the screening length according to (2.3) versus electron concentration.

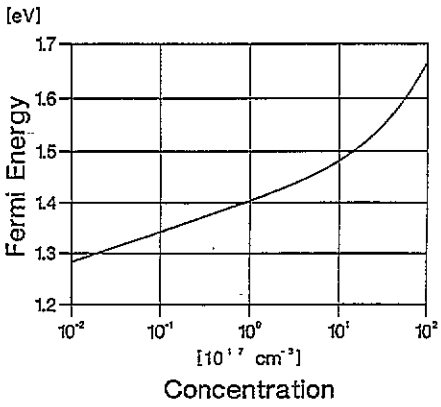

Figure 2. The Fermi level at 300 K versus electron concentration.

The electron temperature in valley i is determined by

$$T_i = \frac{2}{3k_B}\left(\sum_{j=1}^{N_i} w_{ij}/N_i - \frac{1}{2}m_i^* v_i^2\right). \tag{2.4}$$

Here w_{ij} is the energy of the jth electron in valley i, N_i the number of electrons in valley i, m_i^* the effective mass in valley i, and v_i the mean electron velocity in valley i. Equation (2.4) only holds for electrons that are Boltzmann distributed.

The theory developed in [1] directly leads to the plasma frequency of a system of electrons having different effective masses. One arrives at

$$\omega_{pl}^2 = \frac{e^2}{\varepsilon_\infty \varepsilon_0}\sum_{i=1}^{3}\frac{n_i}{m_i^*}. \tag{2.5}$$

ω_{pl} is the plasma frequency and ε_∞ the relative dielectric constant including the polarization of the valence electrons. The meaning of the other variables is the same as above.

The electron distribution in thermal equilibrium is taken to be a Fermi distribution. The number of free electrons and the number of ionized impurities are set equal in our calculations.

3. Electron–electron collisions

3.1. Derivation of the scattering rates

Our description of electron–electron collisions is based on the semiclassical electron model, which implies that electrons can be described by wave packets with a finite extension smaller than the crystal volume. To simplify our calculations, the bands are treated as being parabolic. Also, the cell periodic part of the electron wave function is set to unity. We adopt the theory of scattering of identical particles presented e.g. in [13]. The Hamilton operator for the two electrons in the effective mass approximation is

$$\left(-\frac{\hbar^2}{2m_1^*}\Delta_1 - \frac{\hbar^2}{2m_2^*}\Delta_2 + V(r_1 - r_2)\right)\Psi(r_1, r_2) = E\Psi(r_1, r_2). \tag{3.1}$$

m_i^* is the effective mass of electron i, Δ_i is the Laplace operator for electron i, and V is the interaction potential according to

$$V(r_1 - r_2) = \frac{-e}{4\pi\varepsilon_0\varepsilon_\infty}\frac{\exp(-\beta|r_1 - r_2|)}{|r_1 - r_2|}.$$

Equation (3.1) is transformed by introducing relative coordinates:

$$r = r_1 - r_2 \qquad R = \frac{(m_1^* r_1 + m_2^* r_2)}{(m_1^* + m_2^*)}. \tag{3.2}$$

The scattering problem is now formulated by

$$(-(\hbar^2/2m)\Delta + V(r))\varphi(r) = E_r\varphi(r) \tag{3.3}$$

with

$$m = m_1^* m_2^*/(m_1^* + m_2^*) \qquad E_r = \hbar^2 k_r^2/2m \qquad k_r = (m_2^* k_1 - m_1^* k_2)/(m_1^* + m_2^*).$$

We now suppose that the wave functions of the electrons overlap. Solutions then have the form

$$\varphi(r) = (1/V^{1/2})(e^{ik_r z} + f(\vartheta)e^{ik_r \cdot r}/r). \tag{3.4}$$

V is the volume of the electron wave function. We choose the z-axis to point in the direction of k_r. If we want to obtain the total scattering rate of one of the two colliding electrons, we must divide the result obtained from (3.4) by two. Since electrons have a spin of $\frac{1}{2}$, the colliding electrons form singlet or triplet states. We obtain for the differential cross section of unpolarized particles according to [13]

$$d\sigma/d\Omega = f(\vartheta)^2 + f(\pi - \vartheta)^2 - f(\vartheta)f(\pi - \vartheta). \tag{3.5}$$

$f(\vartheta)$ is real in the first order of Born's approximation. The total cross section for one electron reads

$$\sigma_{tot} = \frac{1}{2}\int_{\text{all angles}} \frac{d\sigma}{d\Omega}\, d\Omega \tag{3.6}$$

and the scattering rate is given by

$$\lambda(k_r) = (\hbar k_r/mV)\sigma^{tot}. \tag{3.7}$$

We have in the first order of Born's approximation

$$f(\vartheta) = -\frac{m}{2\pi\hbar^2}\left|\int_V e^{-ik_r' \cdot r} V(r) e^{ik_r \cdot r}\, dr\right|. \tag{3.8}$$

ϑ is the angle between k_r' and k_r. After some calculation, we arrive at

$$\lambda(k_r) = (me^4 k_r n/\pi\varepsilon_0^2\varepsilon_\infty^2\hbar^3 V)(1/(4k_r^2+\beta^2)\beta^2 - [1/8k_r^2(2k_r^2+\beta^2)]\ln[(4k_r^2+\beta^2)/\beta^2]). \tag{3.9}$$

The second term included here is an interference term. Figure 3 shows the scattering rate with and without inclusion of this term versus relative electron wave number. Equation (3.9) only gives a rough estimate of the scattering rate since at relative energies occurring in the electron system considered the first Born approximation is not sufficient. A proper phase shift calculation to obtain λ for scattering of electrons at ionized impurities has been performed in [14]. However, the corrections did not affect the calculated transport properties significantly at 300 K. We thus feel justified in using the rates obtained by (3.9) for the similar electron–electron scattering process.

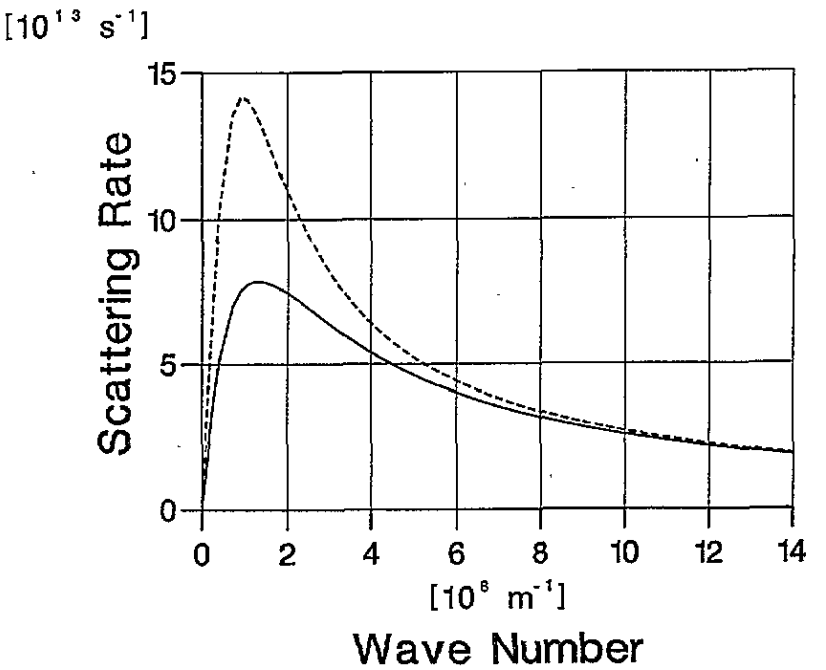

Figure 3. The scattering rate for elastic electron–electron collisions versus relative wave number: $n = 10^{18}$ cm^{-3}. ——, interference term included; – – –, interference term not included.

3.2. Determination of the scattering partners

In transport theory and device simulation, electrons are not considered to be wave packets spread over the entire crystal but to occupy a restricted volume (see, e.g., [15, 16]). The Coulomb force exerted by electrons and ionized impurities beyond the wave function volume is neglected here since we consider a homogeneous crystal having a charge distribution statistically equal to zero. In this approximation, electrons only interact by collisions. We then add a further simplification. Since we want to investigate transport properties of GaAs, which is homogeneous in a statistical sense, the electron distribution is not a function of position. Therefore, the collision partners can be selected from the electron ensemble by

random numbers, thus saving the time to determine the electron positions and to find the spatially nearest neighbours. If the electron volume is set to

$$V = N/n \tag{3.10}$$

with N a natural number and n the electron density, then $N+1$ electrons on average are involved in a scattering process. If k_1 is the wave vector of the scattered electron and if $\{k_i\}$ are the wave vectors of the collision partners, the scattering rate is

$$\lambda(k_1) = \sum_{i=1}^{N} \frac{m_i e^4 |k_r^i|}{\pi \varepsilon_0^2 \varepsilon_\infty^2 \hbar^3 N} \left(\frac{1}{(4k_r^{i2} + \beta^2)\beta^2} - \frac{1}{8k_r^{i2}(2k_r^{i2} + \beta^2)} \ln \frac{4k_r^{i2} + \beta^2}{\beta^2} \right) = \sum_{i=1}^{N} \lambda_i^e(k_1). \tag{3.11}$$

Here interference due to scattering at different electrons is neglected.

Let Γ be the total scattering rate of an electron in a Monte Carlo simulation procedure [17]:

$$\Gamma = \sum_{j=1}^{M} \lambda^j(k_1) + \sum_{i=1}^{L} \lambda_i^e(k_1) + \Gamma_f. \tag{3.12}$$

M is the number of scattering mechanisms without electron–electron collisions, L the number of scattering partners, and Γ_f is the fictitious scattering rate [17]. Our statistical approach requires that L is not a constant but is distributed around N (see (3.10)). We regard this as a minor effect and set $L = N$. We found that simulation results hardly depend on the value of L, as shown in figure 4, where distribution functions calculated with different values of L are compared.

A random number $r (0 \leqslant r \leqslant \Gamma)$ determines the scattering process which actually takes place. If

$$\sum_{j=1}^{M} \lambda^j(k_1) + \sum_{i=1}^{k} \lambda_i^e(k_1) < r < \sum_{j=1}^{M} \lambda^j(k_1) + \sum_{i=1}^{k+1} \lambda_i^e(k_1) \tag{3.13}$$

with

$$0 \leqslant k \leqslant L-1$$

then the electron is scattered at the partner with wave vector k_{k+1}. Further random numbers determine the direction of the relative wave vectors k_r' after the scattering process has taken place. Finally k_1' after the scattering is given by

$$k_1' = k_r' + m_1^*(k_1 + k_{k+1})/(m_1^* + m_{k+1}^*). \tag{3.14}$$

The wave vector of the scattering partner k_{k+1} is left unaltered due to the fact that its end of flight does not coincide with that of the electron with wave vector k_1. This causes momentum and energy to be only statistically conserved in a simulation procedure. This will be discussed in detail in the following section.

3.3. Simulation algorithm

Expression (3.11) can only be evaluated if the momenta of all scattering partners at the moment of the collision are known. To fulfill this condition, we developed an adequate algorithm based on the standard procedure of ensemble Monte Carlo simulation (e.g. [17]).

The total simulation time is divided into equal intervals. Consider a given interval j with time borders t_{j-1}, t_j. The scattering events i for electrons k at times $t_{k,i}$ are computed

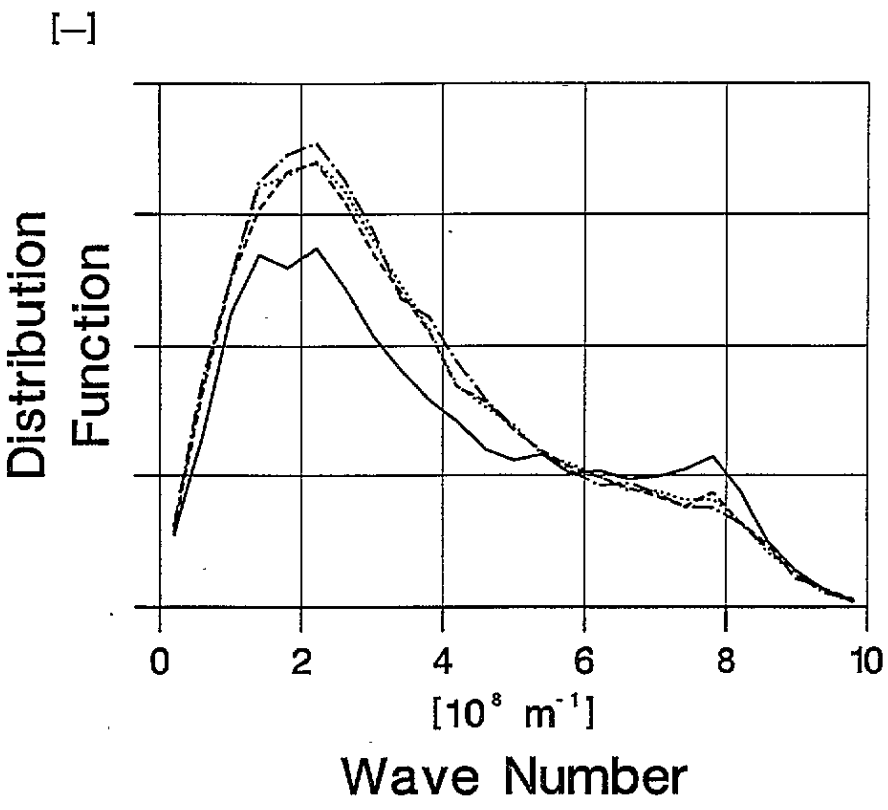

Figure 4. Cuts through distribution functions at $k_L = 0$, $n = 10^{18}$ cm^{-3}, $E = 8$ kV cm^{-1}: ——, without electron–electron collisions; – – –, $L = 1$; · · · · · ·, $L = 5$; — · —, $L = 20$.

for all electrons until $t_{k,i-1} < t_{j-1} < t_{k,i}$. We now continue the simulation of the electron flights in interval j until $t_{k,i} > t_j$ or

$$r > \sum_{j=1}^{M} \lambda^j(k_k). \tag{3.15}$$

The meaning of the symbols in (3.15) is the same as that in equation (3.13). No final state is determined if (3.15) holds. Finally, a fraction of the electrons has traversed the time interval j. The electrons of the remaining fraction are then sorted according to the ends of their flights.

The simulation is continued with the electron having the smallest time of flight. Since the momenta of all other electrons are known at this time, it can be decided whether a fictitious scattering or an electron–electron collision occurs. In the latter case, the scattering partner and the final state are determined as explained in subsection 3.2, and the flight is continued until the electron has traversed the interval or the flight is stopped again because condition (3.15) holds. Then the next of the sorted electrons is simulated.

The procedure is repeated until $t_{k,i} > t_j$ holds for all electrons. We then proceed with the simulation of the electron flights in the next time interval. The algorithm guarantees that the energy is statistically conserved as shown in figure 5. In this figure, results of a simulation neglecting band non-parabolicity are shown. The electrical field is switched on at $t = 0$ ps. If non-parabolicity is generally taken into account but neglected for

electron–electron collisions as required if the method described in section 3.2 is to be used, energy conservation during collisions does not strictly hold (figure 6). However, the relative impact of the collisions on the mean electron velocity remains nearly the same whether non-parabolicity is neglected or not. Hence the small error in the energy balance does not significantly change the results.

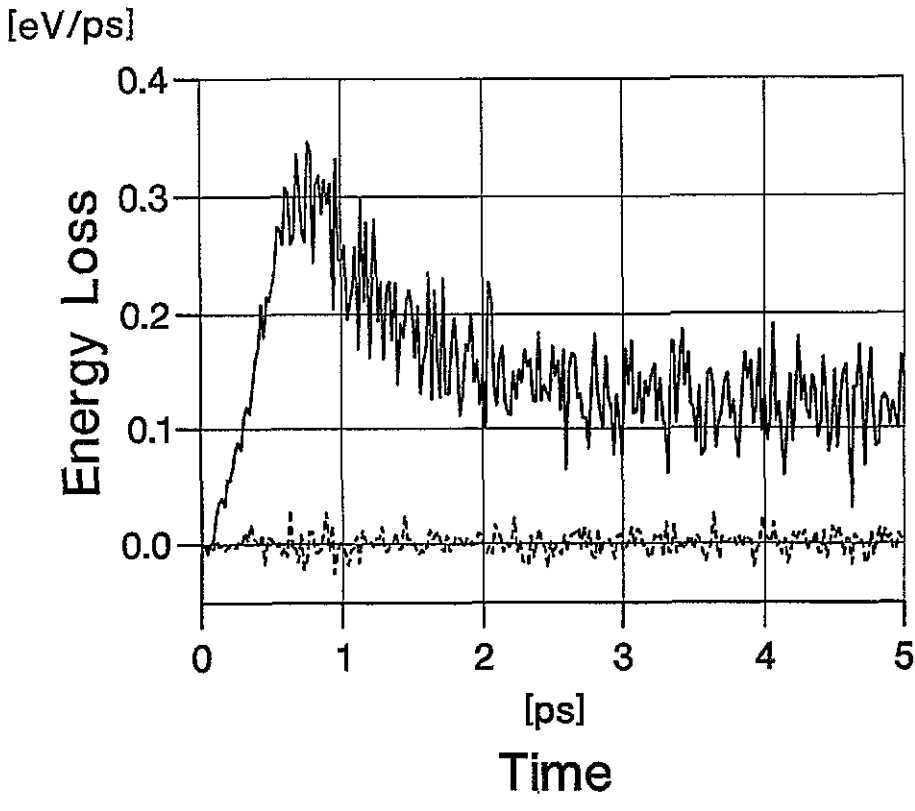

Figure 5. The kinetic energy loss by scattering events at $n = 10^{18}$ cm^{-3} and $E = 10$ kV cm^{-1}. $\alpha_i = 0$. ——, total energy loss; – – –, loss by electron–electron collisions.

The calculation of time-ordered collision events is very time consuming, and in the following a simplification is described. Before simulating electron flights in the interval j (see above), we compute all electron momenta at time t_{j-1}. Now the momenta of the scattering partners are taken from this momentum distribution, which does not change during the time interval. In the stationary case, there is no difference between the distribution at the interval border and the distribution at the moment of a scattering event. In the non-stationary case, a small error occurs, and the energy is not conserved on average. Since we only are interested in stationary results, we apply the simplified method in the following.

3.4. The influence of electron–electron scattering on the distribution function

The influence of collisions on the distribution function depends on the electron concentration and the electric field strength. We briefly discuss here the impact of collisions at $E = 8$ kV cm^{-1}.

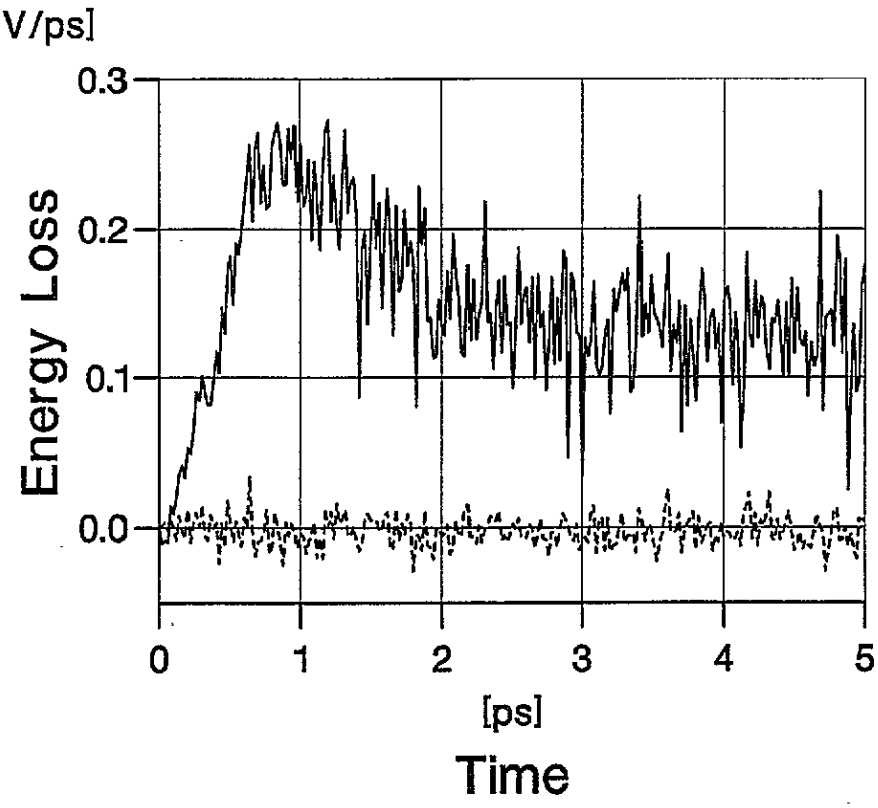

Figure 6. The kinetic energy loss by scattering events at $n = 10^{18}$ cm^{-3} and $E = 10$ kV cm^{-1}. $\alpha_i \neq 0$. ——, total energy loss; – – –, loss by electron–electron collisions.

At $n = 10^{16}$ cm^{-3}, the influence is negligible. At $n = 10^{18}$ cm^{-3}, electron–electron collisions significantly randomize the momenta of the electrons. This effect does not depend significantly on the value of L. Figure 4 shows cuts through distribution functions for $n = 10^{18}$ cm^{-3}, $k_L = 0$, and different values of L (1, 5, 20). The distribution function f is defined such that

$$N_e = \int_{BS} f(k_T, k_L)\, dk_T\, dk_L$$

gives the total number of electrons. k_T is the electron momentum perpendicular to the direction of the electric field, and k_L is the momentum parallel to the field. Evidently, the deviations of the distribution functions for $L = 1$, 5, and 20 at $k_L = 0$ are a second-order effect. In order to reduce statistical fluctuations of the scattering rate (3.11), we set $L = 5$.

3.5. The influence of electron–electron scattering on transport mean values

Figures 7 and 8 show the stationary velocity–field characteristics for electron concentrations of $n = 10^{16}$ cm^{-3} and $n = 10^{18}$ cm^{-3}, respectively, with and without inclusion of electron–electron collision processes. At $n = 10^{16}$ cm^{-3}, the influence of this scattering process on transport properties is negligible. At $n = 10^{18}$ cm^{-3}, however, the stationary peak velocity is raised significantly. This effect also occurs if non-parabolicity is neglected, the energy loss by collisions being statistically exactly equal to zero. A more detailed analysis shows that the mean scattering angle increases with electron concentration, while the mean

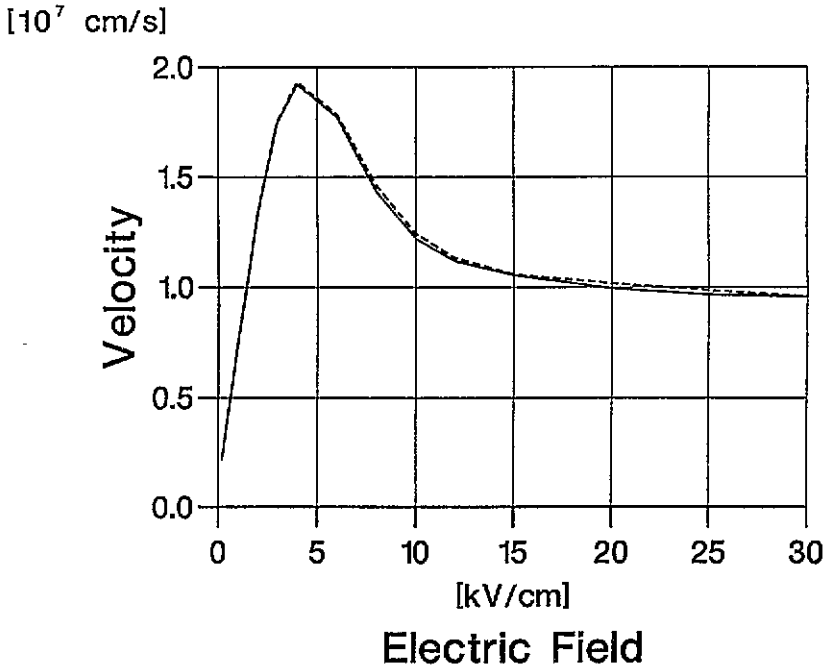

Figure 7. The stationary velocity–field characteristic for $n = 10^{16}$ cm^{-3}: ——, without electron–electron collisions; – – –, collisions included.

scattering rate decreases. We also observe that at $n = 10^{18}$ cm^{-3} the scattering of electrons from the Γ valley to the L valleys is retarded by collisions.

4. The impact of the Pauli exclusion principle on electron transport

Figure 2 shows that the Fermi level shifts at $n \simeq 3 \times 10^{17}$ cm^{-3} into the conduction band. Hence, the Pauli principle affects the distribution function, and some influence of this effect on electron transport is expected.

4.1. The numerical procedure

The simulation conditions cause the distribution function to have axial symmetry with respect to the direction of the electric field vector. We therefore define a two-dimensional distribution function depending on the longitudinal and transverse momenta of the electrons. $f_d(n\Delta k_L, n\Delta k_T, v)$ is by definition equal to the number of electrons in a group of equivalent valleys v with momentum

$$k = (k_L^2 + k_T^2)^{1/2}$$

satisfying

$$\begin{aligned} (m-1)\Delta k_L < k_L < m\Delta k_L \qquad (m \geqslant 1) \\ (n-1)\Delta k_T < k_T < n\Delta k_T \qquad (n \geqslant 1). \end{aligned} \tag{4.1}$$

n and m are natural numbers and $\Delta k_T \Delta k_L$ is the area of a cell in the $k_T - k_L$ plane. The momentum is referred to the centre of a valley. The maximum number M of electrons fulfilling the conditions (4.1) is

$$M(n\Delta k_T, v) = j_v(N/4\pi)(2n-1)\Delta k_T^2 \Delta k_L \qquad (n \geqslant 1) \tag{4.2}$$

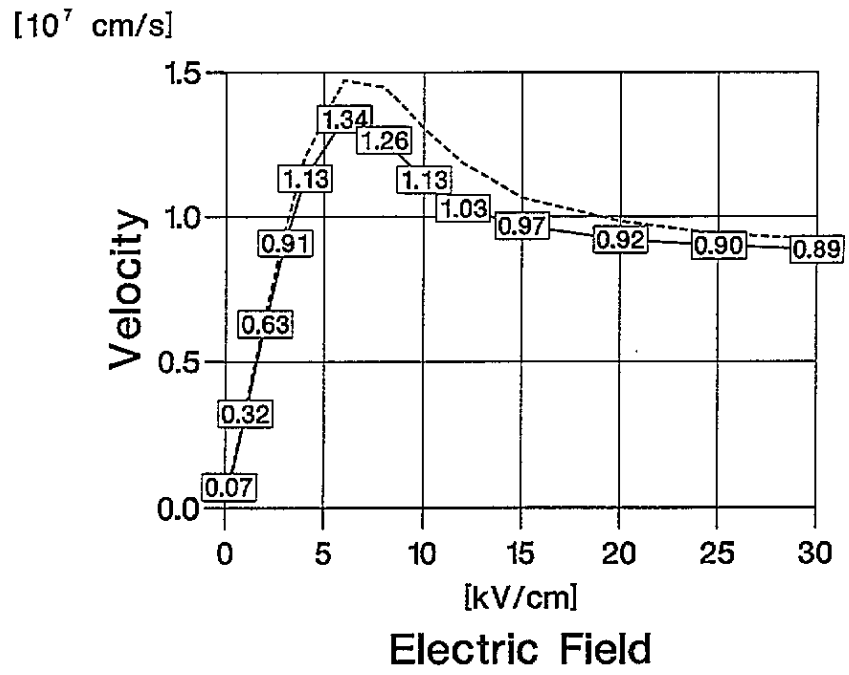

Figure 8. The stationary velocity–field characteristic for $n = 10^{18}$ cm^{-3}: ——, without electron–electron collisions; – – –, collisions included.

with j_v the number of equivalent valleys of type v and N the number of electrons. The probability for any scattering process to end in a cell of the momentum space defined by (4.1) is proportional to

$$M(n\Delta k_T, v) - f_d(n\Delta k_T, m\Delta k_L, v).$$

If the final vector of the scattered electron has been determined in the Monte Carlo procedure, a random number r is chosen according to

$$0 < r < M(n\Delta k_T, v). \tag{4.3}$$

If

$$r > f_d(n\Delta k_T, m\Delta k_L, v) \tag{4.4}$$

the scattering process takes place, otherwise it is annulled and a new time of flight is determined, the electron continuing its flight with the momentum it had just before scattering.

4.2. Numerical results

Figure 9 shows the stationary electron velocity for $n = 10^{18}$ cm^{-3} with and without taking into account the Pauli exclusion principle. Electron–electron collisions are included. The relative rate of forbidden processes at the same concentration is shown in figure 10.

At $n = 10^{16}$ cm^{-3}, the exclusion principle can be neglected. Even at $n = 10^{18}$ cm^{-3} the changes of the stationary mean electron velocity are small. As expected, the electron mobility at low field strengths is raised by the exclusion principle. Since the exclusion principle causes a lowering of the total scattering rate, a larger fraction of electrons gains sufficient energy to be potentially scattered from the Γ valley to the L valleys. Hence the maximum of the $v(E)$-curve is lowered, and $v(E)$ decreases at lower field strengths than it does without inclusion of the exclusion principle. Finally at $E = 30$ kV cm^{-1}, the changes are near the statistical errors of our calculations.

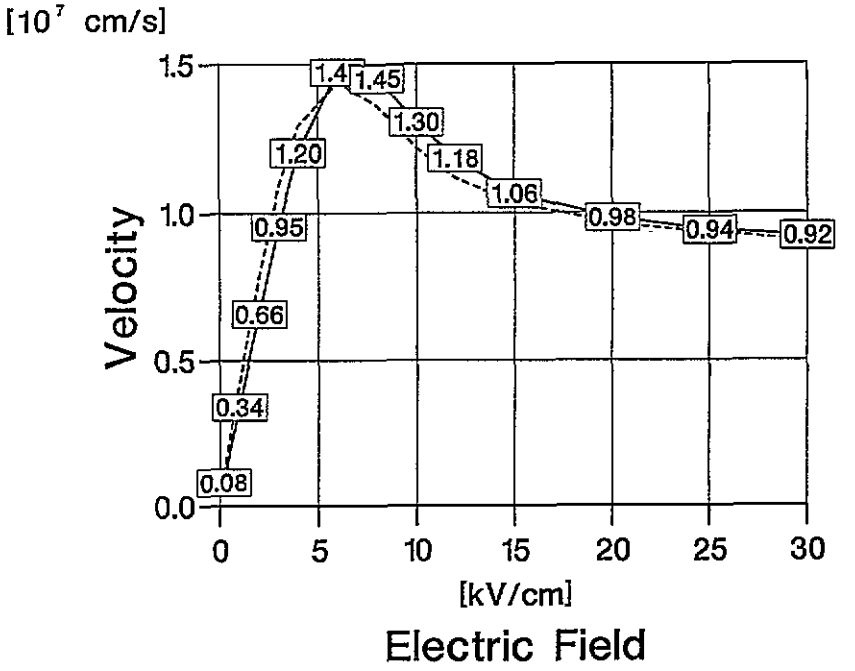

Figure 9. The stationary velocity-field characteristic for $n = 10^{18}$ cm^{-3}: ——, as figure 8, without the exclusion principle; – – –, with the exclusion principle.

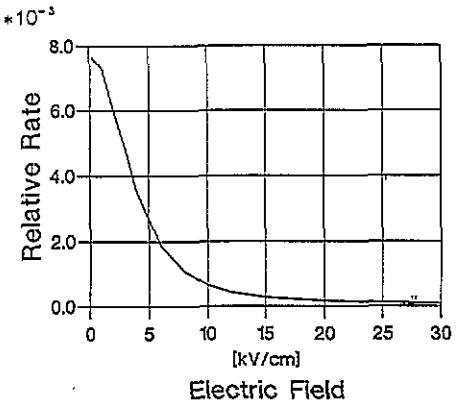

Figure 10. The relative rates of forbidden processes for $n = 10^{18}$ cm^{-3}.

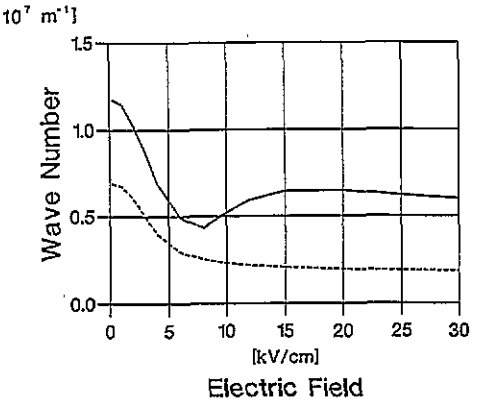

Figure 11. Cut-off wave numbers for the lower mode at $n = 10^{16}$ cm^{-3}: ——, branch 1; – – –, branch 2.

5. Interaction of electrons with coupled plasmon–phonons

5.1. Scattering rates

The derivation of the scattering rates for inelastic scattering of electrons at coupled plasmon–phonons has been presented in [9]. In the latter paper, we neglected the cell periodic part of the electron wave function for simplicity. This approximation is abandoned now to yield results comparable to those of other authors, who generally take overlap integrals into

account [10, 17]. The resulting lengthy expressions for the scattering rates are listed in the appendix.

In the following, we briefly sketch the main results from [9]. Let i be the index of the branch of plasmon–phonons. We then can write for the scattering rate

$$\lambda_{\substack{\mathrm{a}\\(\mathrm{e})}}^{\mathrm{pl-ph},i}(k) = (v_i \lambda_{\substack{\mathrm{a}\\(\mathrm{e})}}^{\mathrm{pl},i}(k) + w_i \lambda_{\substack{\mathrm{a}\\(\mathrm{e})}}^{\mathrm{ph},i}(k))\left(n(\omega_i) + \tfrac{1}{2} \underset{(+)}{-} \tfrac{1}{2}\right). \tag{5.1}$$

Indices a, e denote absorption and emission, respectively, $\hbar\omega_i$ is the energy of a plasmon–phonon, and v_i and w_i are weighting factors for the phononic and plasmonic content of the mode. For $n < 7 \times 10^{17}$ cm^{-3}, $v_i > w_i$ for the low-energy mode and $v_i < w_i$ for the high-energy mode. The lower mode then has plasmonic, the upper mode phononic character. For $n > 7 \times 10^{17}$ cm^{-3}, the character of the modes interchanges.

The magnitude of $\lambda^{\mathrm{pl-ph}}$ depends strongly on the value of the maximum of the oscillation wave number, q_c. This value is determined according to [9] and is given by the point (ω, q_c) where the real part of the electronic part of the dielectric function ε_e and its first derivative are equal to zero. For wave numbers $q > q_c$, no zeros of ε_e occur. For electrons that are Boltzmann distributed, ε_e is given approximately by [3]

$$\varepsilon_e(q,\omega) = \varepsilon_s + \sum_{i=1}^{3} \left(\frac{m_i^*}{2k_B T_i}\right)^{1/2} \frac{e^2 n_i}{\varepsilon_0 \hbar q^3} (Z(\Omega_{1,i}) - Z(\Omega_{2,i})) \tag{5.2}$$

with

$$Z(\Omega) = [\mathrm{i}\pi^{1/2} + (\pi - 2)\Omega]/[1 - \mathrm{i}\pi^{1/2}\Omega - (\pi - 2)\Omega^2]$$

and

$$\Omega_{\substack{1,i\\(2,i)}} = (m_i^*/2k_B T_i)^{1/2}\left(\underset{(-)}{+} \hbar q/2m_i^* + \omega/q\right).$$

The use of (5.2) leads to a small error for q_c at electron concentrations of $n = 10^{18}$ cm^{-3} in thermal equilibrium at $T = 300$ K since degeneracy effects affect the distribution function. In this case, (5.2) yields $q_c = 1.2 \times 10^8$ m^{-1} as compared to the exact result, $q_c = 1.4 \times 10^8$ m^{-1}. As can be inferred from section 4, the influence of degeneracy on the distribution function becomes smaller at higher field strengths, and we continue using (5.2) for the electron concentrations considered here. q_c is determined numerically during a simulation and depends on the relative occupation of the valleys and the electron temperature in the valleys.

Furthermore, we found in [9] another limit for q_c, which for the low-energy mode was shown to be the stronger one. This value is obtained by determining the finite phonon–plasmon lifetime. The finite lifetime is a consequence of damping of an oscillation by energy loss and depends on the electron distribution function.

A first approach to take damping into account is to neglect scattering of electrons at coupled plasmon–phonons of branch i if the lifetime of these excitations is shorter than the interaction time of time dependent perturbation theory. This eventually leads to a smaller cut-off value $q_{c,i}$ for an oscillation branch. The approximation may overestimate the influence of damping. Hence, results obtained without taking damping into account are also discussed.

The screening of the polar optical phonons is treated according to [9].

5.2. The determination of the scattering angle

The scattering angle for scattering of electrons at polar optical phonons is usually determined by the von Neumann procedure [17]. This method requires knowing the maximum of the angular distribution function, $P(\vartheta)$. It is inefficient if there are large regions of ϑ where

$$P(\vartheta) \ll P_{\max} \tag{5.3}$$

holds. $P_{\max}$ denotes the maximum of $P(\vartheta)$. The situation is complicated by plasmon–phonon coupling. Since a maximum q for the coupled modes (a minimum q for the uncoupled phononic mode) introduces a maximum ϑ not equal to π (a minimum ϑ not equal to 0), the usual approximation for $P_{\max}$ cannot be made. Instead of numerically determining $P_{\max}$, and bearing in mind that (5.3) holds for large ϑ, we determine the scattering angle in another way. Let λ be the total scattering rate for a specific scattering process. A random number r between 0 and λ is chosen, and the scattering angle ϑ_s is determined from

$$r = \int_{\vartheta_{\min}}^{\vartheta_s} P(\vartheta) \sin\vartheta = Q(\vartheta_s) \tag{5.4}$$

with

$$P(\vartheta) = \int_0^{2\pi} \int_0^{\infty} S(k, k') k'^2 \, \mathrm{d}k' \, \mathrm{d}\varphi$$

given analytically in the appendix. Since it is impossible to solve (5.4) for ϑ_s, ϑ_s is numerically determined by a searching procedure. First, we set

$$\vartheta_s = (\vartheta_{\max} - \vartheta_{\min})/2. \tag{5.5}$$

If $Q(\vartheta_s) > r$, we set $\vartheta_{\max} = \vartheta_s$, else $\vartheta_{\min} = \vartheta_s$ to obtain a better estimate of ϑ_s by (5.5). This procedure is repeated until

$$\vartheta_{\max} - \vartheta_{\min} < \mathrm{d}\vartheta$$

$\mathrm{d}\vartheta$ being an appropriate lower limit. In our calculations, a value of 0.5° has been used.

5.3. The impact of electron scattering at coupled plasmon–phonons on electron transport

At $n = 10^{16}$ cm^{-3}, scattering occurs only due to the lower mode. The scattering rate for scattering at the high-energy mode is equal to zero. Figure 11 shows the cut-off wave numbers for both modes. The value for the lower mode is lowered by damping. As the electron temperature increases and the L and X valleys become occupied with increasing field strength, damping becomes more effective, and the cut-off value becomes smaller. This results in a mean relative scattering rate, which diminishes with increasing field strength and is equal to zero at $E = 6$ kV cm^{-1}, as can be seen from figure 12. Even for $E < 6$ kV cm^{-1}, the relative scattering rate is smaller than 0.1%, and the impact of this scattering process on the stationary electron velocity can be neglected for $n = 10^{16}$ cm^{-3}. If plasmon damping is neglected and a q_c determined from (5.2) is used, the calculated mean electron velocity is also not influenced.

At $n = 10^{18}$ cm^{-3}, the mean scattering rate for scattering at the low-energy mode is equal to zero for all field strengths. Scattering is only caused by the high-energy mode. Figure 13 shows the cut-off wave numbers for both modes. The value of the low-energy mode is affected by plasmon–phonon damping. In figure 14, the relative scattering rate for the high-energy mode is compared with the polar optical phonon scattering rate, which can be seen to be much higher. Hence the velocity–field characteristic shown in figure 15 is not strongly affected. If damping is neglected, the resulting velocity changes by less than 10%, as can be seen in figure 15.

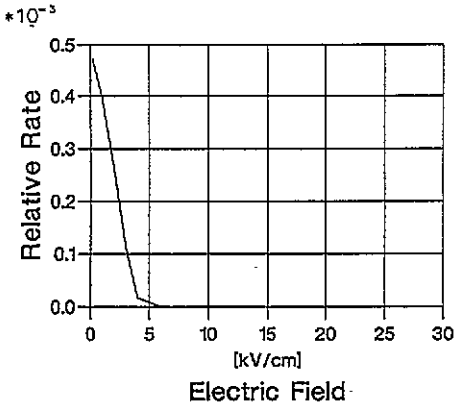

Figure 12. Relative scattering rates for scattering of electrons at plasmons for $n = 10^{16}$ cm^{-3}.

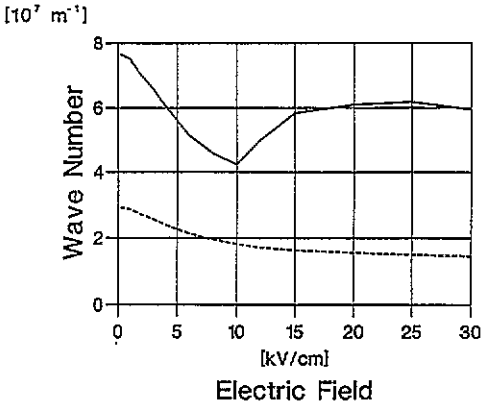

Figure 13. Cut-off wave numbers at $n = 10^{18}$ cm^{-3}: ——, branch 1; – – –, branch 2.

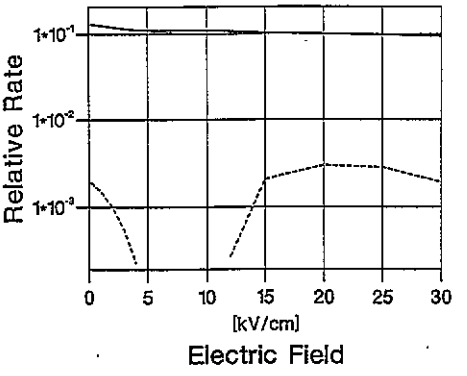

Figure 14. Relative scattering rates at $n = 10^{18}$ cm^{-3}: ——, scattering of electrons at uncoupled polar optical phonons; – – –, scattering of electrons at coupled plasmon–phonons, upper mode.

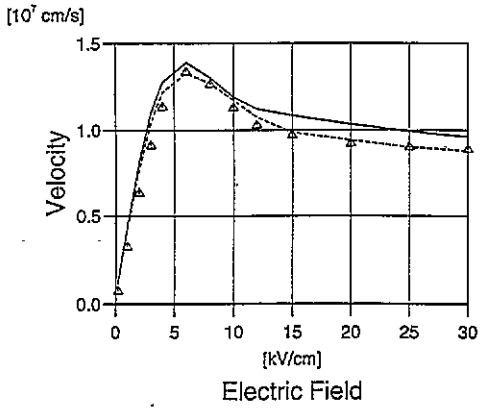

Figure 15. The stationary velocity–field characteristic for $n = 10^{18}$ cm^{-3}: ——, all discussed effects included without damping; – – –, all discussed effects included with damping; Δ, all discussed effects neglected.

6. Discussion of the results

Experimental results that can be compared to our computations are mobility measurements and $v(E)$ characteristics. The mobility is defined here by

$$\mu = \partial v / \partial E$$

and computed for $E = 0.2$ kV cm^{-1}. It is well known that at low field strength a large statistical error of μ remains. To reduce this error, 90 000 electrons were used to calculate mobilities. Measured values can be taken from [18–20]. In these publications, measurements of different authors are quoted.

Experimental and theoretical results can only be compared if the compensation ratio r is known. If n_a is the concentration of ionized acceptors and n_d the concentration of ionized donors, r is given by

$$r = (n_a + n_d)/n.$$

In n-GaAs, $r \neq 1$. A further difficulty arises at high electron concentrations since scattering at neutral impurities cannot necessarily be neglected. Both effects are neglected here, and r is generally set to unity.

The mobility we obtain at 10^{16} cm^{-3} for $r = 2$ coincides nearly exactly that quoted in [22], $\mu = 6.7 \times 10^3$ cm^2 V^{-1} s^{-1}. We checked that our result does not depend on the plasmon cut-off wave number up to $q_c = \beta$. The effects considered do not affect the mobility at $n = 10^{16}$ cm^{-3}, and hence they cannot be the reason for any discrepancies between experiment and theory.

At $n = 10^{18}$ cm^{-3}, the measured mobility taken from [20] is $(2.8 \pm 0.5) \times 10^3$ cm^2 V^{-1} s^{-1}. Neglecting all effects discussed and setting $r = 1$, we obtain $(3.5 \pm 0.5) \times 10^3$ cm^2 V^{-1} s^{-1}. If undamped plasmons are taken into account, we also obtain 3.5×10^3 cm^2 V^{-1} s^{-1}. Screening of the polar optical phonons raises the mobility (see [20]), but this effect is compensated by the additional plasmon scattering process. Inclusion of electron–electron collisions lowers the mobility to $(3.3 \pm 0.5) \times 10^3$ cm^2 V^{-1} s^{-1}. This slight lowering of the mobility has also been observed in [20]. Finally, the Pauli principle raises the mobility to $(3.6 \pm 0.5) \times 10^3$ cm^2 V^{-1} s^{-1}. As also observed in [20], the theoretical mobility at $n = 10^{18}$ cm^{-3} exceeds the experimentally observed value. However, plasmon interaction cannot be the reason for this discrepancy, and the shortcoming has to be searched for elsewhere.

We note that in [21] theoretical mobilities agree with experimental ones in Si by use of a cut-off wave number of β for plasmons at $n = 10^{18}$ cm^{-3}. The relative influence of the plasmon scattering process in Si at $n = 10^{18}$ cm^{-3} and low field strengths may be greater than in GaAs since the plasmon scattering is not partly compensated by screening of polar optical phonons. Furthermore, in GaAs the cut-off wave number at $n = 10^{18}$ cm^{-3} and low field strengths is only $\simeq 0.7\beta$ according to the analysis of the dielectric function.

At $n = 10^{19}$ cm^{-3}, the theoretical mobility neglecting all effects discussed is $(3.3 \pm 0.5) \times 10^3$ cm^2 V^{-1} s^{-1}. This is higher than that obtained in [20], since we neglect the Pauli principle even in computing the screening length. Therefore, the impact of impurity scattering is underestimated. Taking plasmon–phonon interaction and electron–electron interaction into account, we obtain $(4.2 \pm 0.5) \times 10^3$ cm^2 V^{-1} s^{-1} and $(4.0 \pm 0.5) \times 10^3$ cm^2 V^{-1} s^{-1}, respectively. The Pauli principle, however, lowers the mobility drastically to $(0.8 \pm 0.5) \times 10^3$ cm^2 V^{-1} s^{-1}. This is due to the fact that because of forbidden scattering processes in the Γ valley the L valleys are significantly occupied at even very low field strengths. Note that the mobility is now closer to the experimentally observed one but clearly too low. The observed mobilities according to [20] are in the interval $(1.5 \pm 0.3) \times 10^3$ cm^2 V^{-1} s^{-1}.

Measured $v(E)$-curves only exist for materials with high resistivity (about 10^6 Ω cm) and $n \ll 10^{16}$ cm^{-3} [23]. For higher electron concentrations, measurements are still lacking, and a check of our results is not possible at present.

Finally we compare in figure 15 the velocity–field characteristic for $n = 10^{18}$ cm^{-3} including electron–electron interaction and the exclusion principle with the characteristic one obtains by neglecting all these effects. The velocities are changed by less than 10%.

7. Conclusions

We performed Monte Carlo calculations for homogeneous GaAs probes including electron–electron interactions and the Pauli exclusion principle for electron concentrations of $n = 10^{16}$ cm^{-3} and $n = 10^{18}$ cm^{-3} at high electric fields. At $n = 10^{16}$ cm^{-3}, each of these processes can be neglected. For an electron concentration of $n = 10^{18}$ cm^{-3}, the influence

does not exceed 10%. At $n = 10^{19}$ cm^{-3}, a pronounced lowering of the mobility is observed caused by the exclusion principle. Remaining discrepancies to experimental mobility values show that further work is needed.

Acknowledgment

The author thanks the Deutsche Forschungsgemeinschaft for financial support.

Appendix. Scattering rates for scattering of electrons at coupled plasmon–phonons

The scattering probabilities are given by

$$S^{i}_{\substack{\mathrm{a}\\(\mathrm{e})}}(\boldsymbol{k},\boldsymbol{k}') = v_i S^{\mathrm{pl},i}_{\substack{\mathrm{a}\\(\mathrm{e})}}(\boldsymbol{k},\boldsymbol{k}') + w_i S^{\mathrm{po},i}_{\substack{\mathrm{a}\\(\mathrm{e})}}(\boldsymbol{k},\boldsymbol{k}') \tag{A.1}$$

with v_i, w_i weighting factors, see [8],

$$S^{\mathrm{pl},i}_{\substack{\mathrm{a}\\(\mathrm{e})}}(\boldsymbol{k},\boldsymbol{k}') = \frac{e^2\hbar^3}{8V_{\mathrm{g}}\varepsilon_\infty\varepsilon_0 m^{*2}\omega_{\mathrm{pl}}}\left(\frac{k'^2-k^2}{k'^2+k^2-2k'k\cos\vartheta}\right)G(\boldsymbol{k},\boldsymbol{k}')\delta\Big(E(k') - E(k) \underset{(+)}{-} \hbar\omega_i\Big) \tag{A.2}$$

$$S^{\mathrm{po},i}_{\substack{\mathrm{a}\\(\mathrm{e})}}(\boldsymbol{k},\boldsymbol{k}') = \frac{e^2\hbar\omega_{\mathrm{po}}}{2V_{\mathrm{g}}\varepsilon_0}\left(\frac{1}{\varepsilon_\infty}-\frac{1}{\varepsilon_{\mathrm{s}}}\right)\left(\frac{(k'^2+k^2-2k'k\cos\vartheta)}{(q_{\mathrm{c}}^2+k'^2+k^2-2k'k\cos\vartheta)^2}\right)$$
$$\times G(\boldsymbol{k},\boldsymbol{k}')\delta\Big(E(k') - E(k) \underset{(+)}{-} \hbar\omega_i\Big). \tag{A.3}$$

These expressions are derived in [9]. The meaning of the parameters is as follows: V_{g}, crystal volume; ε_∞, high-frequency dielectric constant; ε_{s}, static dielectric constant; m^*, effective mass of the scattered electron; ω_{pl} plasma frequency; ω_{po}, polar optical phonon frequency; ω_i, frequency of the coupled oscillation, branch i; q_{c}, cut-off wave number.

$G(\boldsymbol{k},\boldsymbol{k}')$ is the overlap factor [7]:

$$G(\boldsymbol{k},\boldsymbol{k}') = (a_k a'_k + c_k c'_k\cos\vartheta)^2$$

with ϑ the angle between $\boldsymbol{k}$ and $\boldsymbol{k}'$.

$$a_k = ([1+\alpha E(k)]/[1+2\alpha E(k)])^{1/2} \qquad c_k = (\alpha E(k)/[1+2\alpha E(k)])^{1/2}$$

and α the non-parabolicity factor. We define

$$E' = E \underset{(-)}{+} \hbar\omega_i \qquad \gamma = E(1+\alpha E)$$

$$E(\vartheta) = \gamma + \gamma' - 2\gamma\gamma'\cos\vartheta \qquad D(q_{\mathrm{c}}) = \hbar^2 q_{\mathrm{c}}^2/2m^*.$$

Then

$$P(\vartheta) = v\frac{2^{1/2}}{8\pi}\frac{e^2(m^*)^{1/2}}{\hbar^3\varepsilon_0\varepsilon_\infty\omega_{\mathrm{pl}}}\frac{(\gamma-\gamma')^2(\gamma')^{1/2}}{(1+2\alpha E)}\frac{((1+\alpha E')^{1/2}(1+\alpha E)^{1/2}+\alpha(E'E)^{1/2}\cos\vartheta)^2}{E(\vartheta)}$$
$$+ w\frac{1}{4(2)^{1/2}}\frac{e(m^*)^{1/2}\omega_{\mathrm{po}}}{\pi\varepsilon_0\hbar}\left(\frac{1}{\varepsilon_\infty}-\frac{1}{\varepsilon_{\mathrm{s}}}\right)\frac{(\gamma')^{1/2}}{(1+2\alpha E)}\frac{E(\vartheta)}{(D(q_{\mathrm{c}})+E(\vartheta))}$$
$$\times((1+\alpha E')^{1/2}(1+\alpha E)^{1/2}+\alpha(E'E)^{1/2}\cos\vartheta)^2. \tag{A.4}$$

The minimal (maximal) ϑ is given by the minimal (maximal) $q = |\boldsymbol{k}-\boldsymbol{k}'|$. We define

$$c_{\substack{\min\\(\max)}} = \Big(\gamma+\gamma'-\hbar^2 q_{\substack{\min\\(\max)}}/2m^*\Big)/2(\gamma\gamma')^{1/2}.$$

Then

$$\vartheta_{\substack{\min\\(\max)}} = \begin{cases} 0 & |c_{\substack{\min\\(\max)}}| < 1 \\ \cos^{-1}(c_{\substack{\min\\(\max)}}) & -1 \leqslant c_{\substack{\min\\(\max)}} \leqslant 1. \end{cases}$$

Finally the integral over $P(\vartheta)$ is given by

$$\begin{aligned} Q(\vartheta_s) = vc_{pl}\left(F^2\ln(E(\vartheta)) - 2\alpha F E(\vartheta)\frac{\alpha^2E^2(\vartheta)}{2}\right) \\ + wc_{po}\left(\frac{D(q_c)}{D(q_c)+E(\vartheta)}(F^2+2\alpha D(q_c)F) + \ln(D(q_c)+E(\vartheta))\right. \\ \times (F^2+4\alpha D(q_c)F+3\alpha^2D^2(q_c)) + (D(q_c)+E(\vartheta)) \\ \left.\times(-2\alpha F - 3\alpha^2D(q_c)) + \alpha^2\frac{(D(q_c)+E(\vartheta))^2}{2}\right)\Bigg|_{\vartheta=\vartheta_{min}}^{\vartheta=\vartheta_s}. \end{aligned} \tag{A.5}$$

Here

$$c_{pl} = [e^2(m^*)^{1/2}/32\times 2^{1/2}\pi\hbar^3\varepsilon_0\varepsilon_\infty\omega_{pl}](\gamma-\gamma')^2/(1+2\alpha E)(1+\alpha E)(1+\alpha E')(\gamma)^{1/2}$$

$$c_{po} = [e^2(m^*)^{1/2}\omega_{po}/32\times 2^{1/2}\pi\hbar\varepsilon_0](1/\varepsilon_s - 1/\varepsilon_\infty)/(1+2\alpha E)(1+\alpha E)(1+\alpha E')(\gamma)^{1/2}$$

$$F = 2(1+\alpha E)(1+\alpha E') + \alpha(\gamma+\gamma').$$

$Q(\vartheta_s)$ is used to determine the scattering angle ϑ_s. The total scattering rate is given by $Q(\vartheta_{max})$.

References

[1] Bohm D and Pines D 1953 *Phys. Rev.* **92** 609
[2] Takenaka W, Inoue M and Inuishi Y 1979 *J. Phys. Soc. Japan* **47** 861
[3] Lugli P 1985 *PhD Thesis* Colorado State University
[4] Mansour N S, Diff K and Brennan K F 1991 *J. Appl. Phys.* **70** 6854
[5] Kim M E, Das A and Senturia S D 1978 *Phys. Rev.* B **18** 6890
[6] Buot F A and Jensen K L 1990 *Phys. Rev.* B **42** 9429
[7] Boenig L and Schoenhammer K 1993 *Phys. Rev.* B **47** 9203
[8] Rota L and Lugli P 1989 *Solid State Electron.* **32** 1423
[9] Peschke C 1993 *J. Appl. Phys.* **74** 327
[10] Littlejohn M A, Hauser J R and Glisson T H 1977 *J. Appl. Phys.* **48** 4587
[11] Hintz A 1990 *PhD Thesis* Technische Universität Hamburg–Harburg
[12] Ashcroft N W and Mermin N D 1976 *Solid-State Physics* (Philadelphia, PA: Saunders) ch 17
[13] Messiah A 1985 *Quantenmechanik* vol 2 (Berlin: de Gruyter) ch 14
[14] Meyer J R and Bartoli F J 1981 *Phys. Rev.* B **23** 5413
[15] Ashcroft N W and Mermin N D 1976 *Solid State Physics* (Philadelphia, PA: Saunders) ch 12
[16] Fischetti M V and Laux S E 1988 *Phys. Rev.* B **38** 9721
[17] Fawcett W, Boardman A D and Swain S 1970 *J. Phys. Chem. Solids* **31** 1963
[18] DiLorenzo J V (ed) 1982 *GaAs FET Principles and Technology* (Dedham, MA: Artech) p 71
[19] *Landolt–Börnstein New Series 1982* Group III, vol 17a, ed O Madelung (Berlin: Springer) p 531
[20] Lowney J R and Bennet H S 1991 *J. Appl. Phys.* **69** 7102
[21] Fischetti M V 1991 *Phys. Rev.* B **44** 5527
[22] Look D 1989 *Electrical Characterization of GaAs Materials and Devices* (New York: Wiley) ch 1.3
[23] Ruch J G and Kino G S 1967 *Appl. Phys. Lett.* **10** 40